

Extension of the intranuclear cascade model to neutron-induced nonelastic cross sections in the low-energy region

Masahiro Nakano^{1,2,*} and Yusuke Uozumi²¹*Junshin Gakuen University, Minami Ward, Fukuoka, 815-0036, Japan*²*Kyushu University, Nishi-ku, Fukuoka 819-0935, Japan*
 (Received 27 March 2019; revised manuscript received 18 June 2019; published 30 September 2019)

Two features, a slow slope and a sharp drop, in neutron-induced total nonelastic cross sections in ²⁷Al and ²⁰⁸Pb are analyzed within the framework of an intranuclear cascade (INC) model. First, to reproduce the slow slope from 100 to 10 MeV, the original INC is generalized in two points; a method to construct the ground state of the target nucleus and a method of taking the effective two-body cross sections between two nucleons. Second, to analyze the origin of the sharp drop from 10 MeV to nearly 1 MeV, the INC is extended to include quantum effects which are originated from the existence of the discrete levels in the nuclear potential. It is shown that this extension leads to the sharp drops in the very low energy below around 10 MeV. It is concluded that the INC model can be extended to explain the sharp drops in addition to the slow slope in neutron-induced nonelastic cross sections for ²⁷Al and ²⁰⁸Pb in the energy region from 100 MeV down to 1 MeV.

DOI: [10.1103/PhysRevC.100.034619](https://doi.org/10.1103/PhysRevC.100.034619)

I. INTRODUCTION

Nonelastic cross section is defined as the total reaction cross section minus the elastic cross section. It includes all the reactions such as particle emissions and absorptions except the elastic reaction. Experimental data on the neutron-induced nonelastic cross section are very few because of difficulty of the measurement, especially in the low-energy region below 100 MeV. In Fig. 1, we show the data of ²⁷Al and ²⁰⁸Pb where nonelastic cross sections are relatively well measured in a wide range [1–10]. Although the data have experimental errors, the tendencies of the cross sections are similar to each other. Two common features are clearly observed in the neutron-induced nonelastic cross section in an energy region of less than 100 MeV. It shows a gradually rising slope as the incident energy of neutron becomes small in the energy region from 100 MeV to around 10 MeV, and a sharp drop in a narrow energy range from around 10 MeV to nearly 1 MeV. It is important that the common features are observed in typical heavy and light nuclei; ²⁰⁸Pb and ²⁷Al. Furthermore, partial data of several nuclei ⁶C [9], ²⁶Fe [9,11], ⁸³Bi [7,11] in the energy region around 10 MeV have the same tendency.

The sharp drop below 10 MeV raises one of interesting problems of the neutron-induced nonelastic cross section. If the projectile is proton, the Coulomb interaction between the proton and target nuclei strongly reject the particle injection at the very low energy, then it is natural that the proton-induced reaction cross section sharply drops. The Coulomb barrier, however, cannot affect the neutron.

Concerning nucleon-induced reactions, there have been several dynamic models such as intranuclear cascade model [12], quantum molecular dynamics [13] and antisymmetrized

molecular dynamics [14]. Among them, the intranuclear cascade (INC) model is a remarkable approach to the nuclear reactions. The extensive studies by Liege group have succeeded to explain various experimental data not only for nucleon-induced reactions but also for antiproton, pion, light cluster-induced reactions, and they have shown the INC model can apply various phenomena [[15] and references therein]. Concerning the nonelastic cross sections, their INCL could explain the cross sections in the 10–100 MeV range. Nevertheless, the sharp drop below around 10 MeV in the neutron-induced nonelastic reaction is not well explained [16]. Uozumi group have shown that their INC model followed by the generalized evaporation model (GEM) has explained various reactions such as (p,p'x), (p,dx), and (p,αx) in very wide energies and angles [17–20]; however, they have not applied their INC model to the neutron-induced reaction until now.

Therefore, one of our aims of this paper is to propose one attempt to explain the origin of the sharp drop. The other aim is to generalize the INC model by Uozumi group to reproduce the slow slope from 100 MeV to around 10 MeV.

There has been an opinion generally believed that the INC model based on the classical dynamics cannot be applied to the low-energy region below several tens MeV since the wavelength becomes longer than mean free path of nucleon [21]. However, there are many studies which disprove this opinion. Cugnon *et al.* shows that the INC model is promising in a low-energy region near 40 MeV [22]. Uozumi *et al.* have shown the effectiveness of the INC model in 50 MeV region by an explanation of the (p,p') reaction cross sections. Furthermore, Boudard *et al.* applied the INC model to the energy range from 1 MeV to 2 GeV [16].

After the wavelength becomes longer in the low-energy region, phenomena which happen are ruled by the interference

*nakano@med.uoeh-u.ac.jp

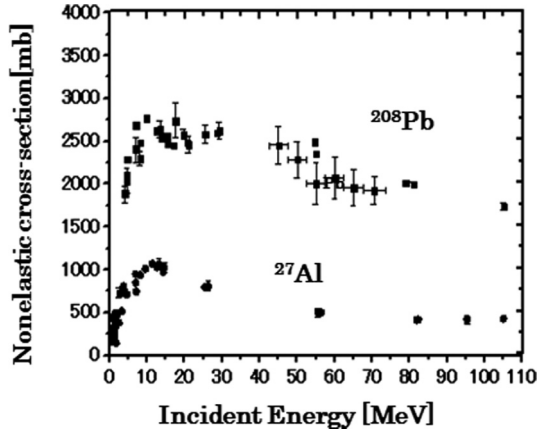


FIG. 1. Experimental data of neutron-induced nonelastic cross sections of ^{27}Al and ^{208}Pb .

of their waves. Kawai discussed on this problem whether the interference is essential or not and concluded that the interference of the outgoing waves generated at different points of the nucleus is canceled out [23]. Therefore, the classical treatment in the INC model makes sense even in the low-energy region. We believe this paper is one of the studies which testify validity of the INC model in the low-energy region.

II. GENERALIZATION OF THE INC MODEL

A. Constitution of the ground state

In the original INC, the ground state is prepared based on a random sampling both on the positions and momentums. On the positions of the particles in the nucleus, we use a random number method to reproduce the Wood-Saxon density distribution as a whole in a probabilistic way. The densities of the nucleons in the ground states are shown in Fig. 2 for ^{27}Al and ^{208}Pb . However, the distribution of momentum in the original INC model is randomly chosen to reproduce a uniform distribution which is shown by the dashed line in Fig. 3. The total cross sections calculated using this ground state of the random sampling bring a peak around $E_{\text{in}} = 40$ MeV both for

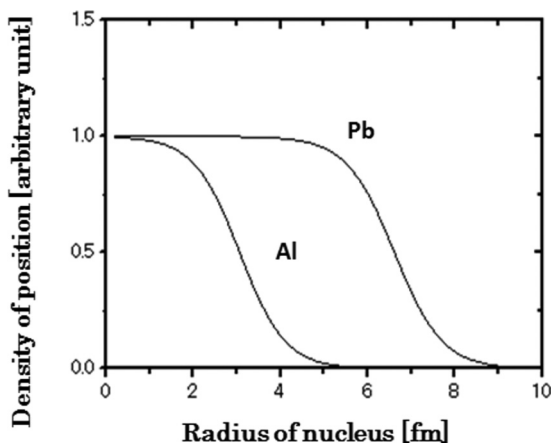


FIG. 2. Distributions of positions of nucleons in the ground states for ^{27}Al and ^{208}Pb . Wood-Saxon shape is realized as a whole.

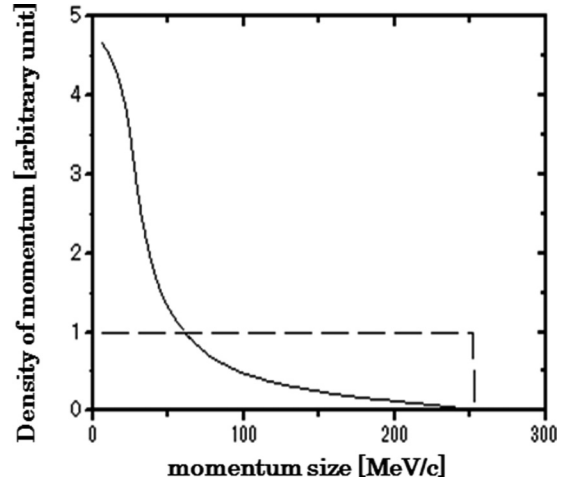


FIG. 3. Distributions of momentum in the ground states, which are the same for ^{27}Al and ^{208}Pb . The original INC model gives the uniform distribution (dashed line), however, the local dependent momentum method gives a sharply damped distribution (solid line).

Al and Pb which is shown by the broken lines in Fig. 4. The tendency is quite different from the experimental data.

In this work, we generalize the uniform ground state to a new ground state based on a local dependent momentum method. On the positions, the same procedure is given by the random setup as the original INC model. However, the momenta are prepared according to the effective nucleon mass at the particle position. The effective nucleon mass is determined by a local dependent formula,

$$M^*(r) = M + U(r), \quad (1)$$

where M is the nucleon mass and the potential $U(r)$ has a Wood-Saxon shape as follows:

$$U(r) = V_0/[1 + \exp(r - r_0)/a_0]. \quad (2)$$

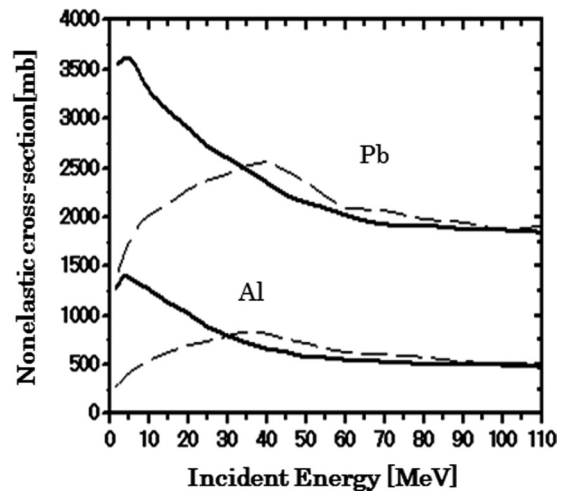


FIG. 4. Neutron-induced nonelastic cross sections calculated with the ground state constructed by random method (broken line) and by the new method (solid line). The same two nucleon cross sections in Eqs. (6)–(8) are taken for both calculations.

TABLE I. Wood-Saxon parameters, the radius r_0 and the diffuseness a_0 for two targets ^{27}Al and ^{208}Pb .

	r_0 [fm]	a_0 [fm]
^{27}Al	2.840	0.569
^{208}Pb	6.620	0.546

In this paper, the parameters r_0 and a_0 of the Wood-Saxon are chosen from the experimental data of charge distribution by electron scattering experiments [24], which are given in Table I.

Using this effective nucleon mass, the maximum momentum at r is given by

$$P_{\max}(r) = \sqrt{E_f^2 - M^*(r)^2}, \quad (3)$$

where E_f is the Fermi energy given by the nucleon mass minus the binding energy, i.e., $E_f = 938.93 - 8.74$ MeV in this paper. The momentum of particles is determined by

for pp

$$\begin{aligned} S &= 41 + 60(P_G - 0.9) \exp(-1.2P_G) && \text{for } 1.5 \text{ GeV}/c < P_G < 5 \text{ GeV}/c, \\ S &= 23.5 + 24.6 / \{1 + \exp[-(P_G - 1.2)/0.1]\} && \text{for } 0.8 \text{ GeV}/c < P_G < 1.5 \text{ GeV}/c, \\ S &= 23.5 + 1000(P_G - 0.7)^4 && \text{for } 0.4 \text{ GeV}/c < P_G < 0.8 \text{ GeV}/c, \\ S &= 34(P_G/0.4)^{-2.104} && \text{for } P_G < 0.4 \text{ GeV}/c, \end{aligned} \quad (4)$$

for np

$$\begin{aligned} S &= 42 && \text{for } P_G > 2 \text{ GeV}/c, \\ S &= 24.2 + 8.9P_G && \text{for } 1 \text{ GeV}/c < P_G < 2 \text{ GeV}/c, \\ S &= 33 + 196 \text{abs}(P_G - 0.95)^{2.5} && \text{for } 0.4 \text{ GeV}/c < P_G < 1 \text{ GeV}/c, \\ S &= 6.3555P_G^{-3.2481} \exp[-0.377(\ln P_G)^2] && \text{for } P_G < 0.4 \text{ GeV}/c, \end{aligned} \quad (5)$$

where P_G is the relative momentum of the two nucleons in the unit of GeV/c.

The two-body cross sections of the improved Cugnon has defects, i.e., there are jumps in the curvature at each edge point since they are separately given for each interval. Furthermore, the INC model calculations using the improved two-body cross sections by Cugnon largely overestimate the data as shown in Fig. 6. Therefore, we introduced a new set of effective two-body cross sections. In the calculations of ^{208}Pb and ^{27}Al , we used the same two-body cross sections. The expression is not unique since many formulas can represent a similar shape. One formula is given for $P_G < 2$ GeV/c as follows:

$$S = (Y1 + Y2)(0.55 + 0.45 / \{1 + \exp[-(P_G - 0.7)/0.07]\}) + 0.20Y3, \quad (6)$$

random numbers, which are chosen in a probabilistic way from zero to the maximum momentum $P_{\max}(r)$. As a result, the new ground state has a sharply damped distribution as shown by the solid line in the Fig. 3. It gives smaller momentum in a peripheral region of the nucleus. As is shown by the solid line in Fig. 4, the calculation gives completely different curvature from the result of the uniform distribution; a slow slope as the incident energy goes to small. This result indicates that the local dependent distribution should be selected instead of the uniform distribution.

B. Effective two-body cross sections between two nucleons

Cugnon *et al.* [25] introduced improved two-body cross sections given by following equations for better fits to low-energy phenomena. They insist that these cross sections were made to reproduce the free NN cross sections, and is valid down to $P_G = 0.1$ GeV/c. The two-body cross sections give a sufficient fit, especially to higher energy phenomena. The two-body cross sections S [mb] are expressed by the following equations for each energy interval:

where the functions $Y1$, $Y2$, and $Y3$ are functions given as follows:

for pp

$$\begin{aligned} Y1 &= 250 \exp(-P_G^{1.2}/0.1), \\ Y2 &= 26.5 / \{1 + \exp[-(P_G - 1.178)/0.122]\} + 22, \quad (7) \\ Y3 &= 3300 \exp(-P_G^{0.8}/0.07) \\ &\quad + 80000 \exp(-P_G^{0.86}/0.02), \end{aligned}$$

for np

$$\begin{aligned} Y1 &= 67 \exp[-(P_G - 0.12)^2/0.15], \\ Y2 &= (10P_G + 23) / \{1 + 0.4 \exp[-(P_G - 0.6)/0.115]\}, \\ Y3 &= 8000 \exp(-P_G/0.072). \end{aligned} \quad (8)$$

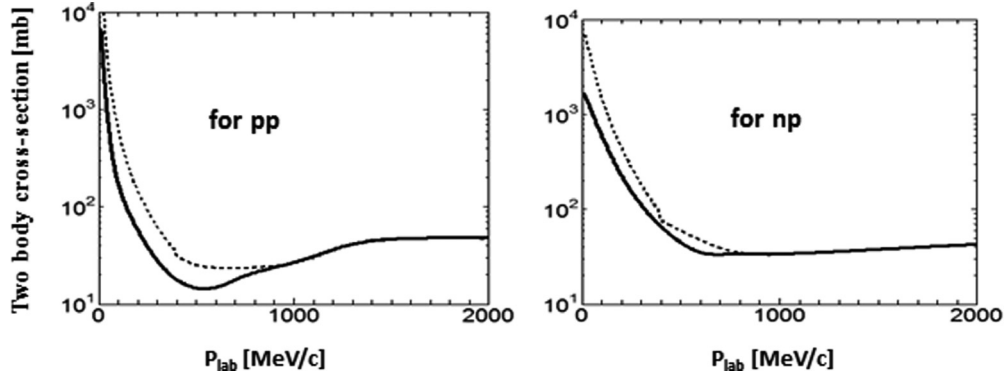


FIG. 5. Two-body reaction cross section for pp (left) and pn (right) by the improved Cugnon (dashed line) in Eqs. (4) and (5) and the proposed one (solid line) in Eqs. (6)–(8).

As illustrated in Fig. 5, the proposed two-body cross sections are similar to those to the improved Cugnon *et al.* Our two-body cross sections are slightly smaller than those by the improved Cugnon in the momentum range smaller than $P_G < 1$ GeV/c. This implies that the free cross sections should be reduced as a result of the medium effects in the nuclear matter.

The calculated result based on the two generalizations reproduces the slow slope in the experimental data as is shown in Fig. 6. However, it cannot reproduce the sharp drop below around 10 MeV. The slow slope of the calculated cross-section results from the fact that the two-body cross sections are sharply rising in the low energy as shown in Fig. 5. Hence, it is obvious that a further extension is necessary for the generalized INC to describe the sharp drop of the experimental data in the low energy less than around 10 MeV.

III. EXTENSION OF THE INC MODEL

The INC model is based on classical dynamics. Then there is a limitation of a classical model, that is, a simple model usually cannot include quantum effects. There is an important quantum effect, i.e., effects originated from Pauli principle. In

the original INC model, the effects have been already included effectively by the treatment that the process is forbidden if the energy of a scattered particle is below the Fermi sea. The importance of the Pauli principle is also pointed out in a phenomenological model [26].

In very low energies, there is another important quantum effect, that is originated from the existence of discrete levels. In quantum mechanics, scattered particles should lead to the target excitations of discrete levels. We call this effect as “discrete level constraint.” Following this constraint, the allowed phase space in the energies of the scattered particles is going to zero when the particle energy goes to zero since the allowed levels becomes sparse in the very low energies. From this sense, the traditional treatment of INC that postulates the continuous states over the Fermi sea is not proper. We simulate this effect as a transition probability. The transition in energy of scattered two particles is

$$E1 + E2 \rightarrow E1' + E2'. \quad (9)$$

The momentum and energy are conserved in the INC model after a collision, so that $E1 + E2 = E1' + E2'$.

The transition probability of the two nuclei is the multiplication of the probabilities of two nucleons:

$$P(E1', E2') = P(E1')P(E2'). \quad (10)$$

We determined originally the probability $P(E)$ using the level energies and the widths of the several single particle orbits in the shell model. This approach succeeded to reproduce the experimental data; however, determining the many parameters is cumbersome since the parameters are dependent on the individual target. Instead, in this paper we simplify the condition by introducing the following shape of the transition probability:

$$P(E) = 1/\{1 + \exp[-(E_0 - E)/w]\}. \quad (11)$$

The function of $P(E)$ is called a sigmoid curve, which is smooth curve from 0 to 1. For parameters in Eq. (11), we set $E_0 = (E_i + E_f)/2$ and $w = 1.1$ MeV for both nuclei. Note that the energy E_0 is the middle point of E_i and E_f , then the probability is 1/2 at $E = E_0$. The $P(E)$ has features that it approaches to 0 as E goes to E_i and to 1 as E goes to E_f . For our problem, we should set $E_i = E_{\text{Fermi}}$ (Fermi energy) and $E_f = M$ (nucleon mass) for neutron, and M (nucleon

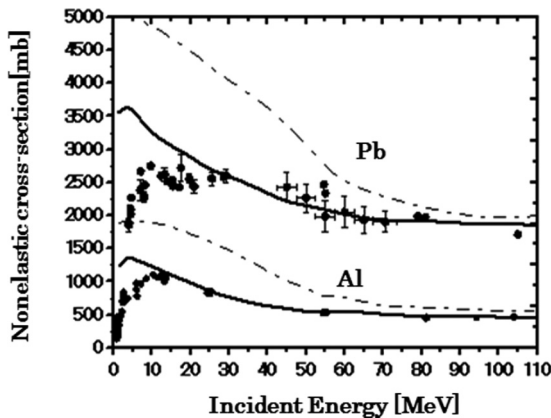


FIG. 6. Comparison between the Experimental data (dots) and two results by using the improved two-body cross sections (dash-dotted lines) in Eqs. (4) and (5) and by the proposed cross sections (solid lines) in Eqs. (6)–(8) for ^{27}Al and ^{208}Pb .

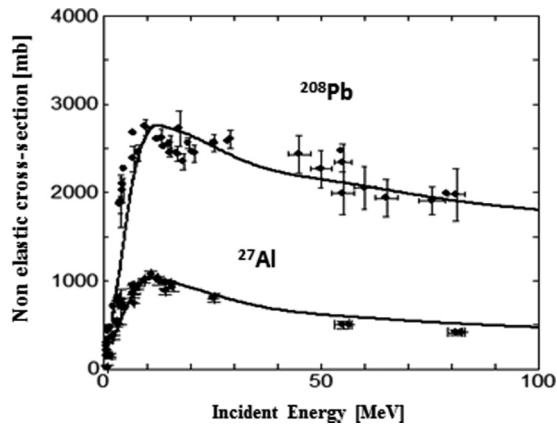


FIG. 7. Comparison between the Experimental data (dots) and the calculated result by the extended INC (solid lines) for ^{27}Al and ^{208}Pb .

mass) + Coulomb barrier for proton. The Fermi energy is set to be 938.92 MeV (nucleon mass) -8.74 MeV (binding energy) for both nuclei, and Coulomb barrier is 3.30 MeV for ^{27}Al , and 8.92 MeV for ^{208}Pb , respectively. It is noted that the essential feature of the sharp drop does not largely depend on the detail of the parameters. We require that two nucleons having the energies E_1' and E_2' follow the probability distribution $P(E_1', E_2')$ as a whole. The process is forbidden when the two nucleon transitions do not follow the transition probability. It should be stressed that this condition is different from the Pauli blocking which is generally used. The Pauli blocking condition works for nucleons in the energy range of $E < E_{\text{Fermi}}$, however, the bound-state constraint does in the energy range of $E > E_{\text{Fermi}}$.

IV. RESULTS AND DISCUSSIONS

The INC model as extended in this way describes excellently the sharp drops both in ^{208}Pb and ^{27}Al , as shown in Fig. 7. The reason of the discrepancy between the generalized INC by the solid lines and the experimental data in Fig. 6 is now clear. The origin of the sharp drop is from the quantum effect. The fact that the scattered two particles should go to the discrete bound states confines the phase space in energy of the two

nucleons. The phase space goes to narrow as the energy of the induced neutron goes to small.

In the case of the large injection energy, the scattered nucleon inside the nucleus goes up to a sufficiently high energy than the free energy, then $P(E_i') = 1$. In this case, there are no restrictions, then a classical model works effectively. However, in the case of a very low injection energy, the particle moves to a little over Fermi sea, and the energy of the injected neutron goes down near the Fermi sea, where the transition probability $P(E_i')$ is nearly zero since there is no allowed state. This means that most of these transitions cannot be allowed. This leads to the sharp drop in the cross sections in very low energy.

V. CONCLUSIONS

We have generalized the original INC model in two points; the ground state and the two-nucleon cross sections, and these generalizations bring a fit to the slow slope in the neutron-induced cross sections. In addition to these two generalizations, we further extend the INC to include the effect originated from the existence of bound states.

There are two quantum effects in the INC model. The one is the effects from Pauli principle, which has been already included in the original INC model. The other quantum effect is newly included one which is originated from “discrete level constraint.” The origin of the sharp drop is that the allowed phase space of scattered two nucleons becomes narrow as the energy of the induced neutron goes to very low. It is noted that this effect is confined in the very low energy, then the original INC works well in a wide range of high-energy region.

Through our analysis, conclusions are: (1) the slow slope from 100 MeV to around 10 MeV is reproduced by two generalizations; (2) the sharp drops of the nonelastic reaction cross section in very-low-energy region below around 10 MeV is explained by the quantum effect due to the existence of discrete levels; (3) finally, the INC model can be extended to include the quantum effect, and by the appropriate inclusion of the effect, the INC model can reproduce the experimental data for two nuclei of ^{27}Al and ^{208}Pb .

ACKNOWLEDGMENT

We are grateful for Dr. Yuji Yamaguchi and Dr. Gaku Watanabe, who continuously supported this work.

- [1] J. R. Beyster, R. L. Henkel, R. A. Nobles, and J. M. Kister, *Phys. Rev.* **98**, 1216 (1955).
- [2] M. H. MacGregor, W. P. Ball, and R. Booth, *Phys. Rev.* **111**, 1155 (1958).
- [3] Ju. G. Degtjarev, *J. Atomnaya Energiya* **19**, 456 (1965).
- [4] Ju. G. Degtjarev and V. G. Nadochij, *J. Atomnaya Energiya* **11**, 397 (1961).
- [5] M. Ibaraki, M. Baba, T. Miura, T. Aoki, T. Hiroishi, H. Nakashima, S. Meigo, and S. Tanaka, *J. Nucl. Sci. Tech. sup.* **2**, 405 (2002).
- [6] R. G. P. Voss and R. Wilson, *Proc. Roy. Soc. (London) A* **236**, 41 (1956).
- [7] T. W. Bonner and J. H. Slattery, *Bull. Am. Phys. Soc. Ser. II* **1**, 175 (1956).
- [8] W. P. Ball, M. H. MacGregor, and R. Booth, *Phys. Rev.* **110**, 1392 (1958).
- [9] H. L. Taylor, O. Lönsjö, and T. W. Bonner, *Phys. Rev.* **100**, 174 (1955).
- [10] A. H. Armstrong and Glenn M. Frye, Jr., *Phys. Rev.* **103**, 335 (1956).
- [11] J. R. Beyster, M. Walt, and E. W. Salmi, *Phys. Rev.* **104**, 1319 (1956).
- [12] R. Serber, *Phys. Rev.* **72**, 1114 (1947).
- [13] J. Aichelin and H. Stöcker, *Phys. Lett. B* **176**, 14 (1986).

- [14] A. Ono, H. Horiuchi, T. Maruyama, and A. Ohnishi, *Prog. Theor. Phys.* **87**, 1185 (1992).
- [15] J. L. Rodriguez-Sanchez, J.-C. David, D. Mancusi, A. Boudard, J. Cugnon, and S. Leray, *Phys. Rev. C* **96**, 054602 (2017).
- [16] A. Boudard, J. Cugnon, J.-C. David, S. Leray, and D. Mancusi, *Phys. Rev. C* **87**, 014606 (2013).
- [17] Y. Uozumi, Y. Sawada, A. Mzhavia, S. Nogamine, H. Iwamoto, T. Kin, S. Hohara, G. Wakabayashi, and M. Nakano, *Phys. Rev. C* **84**, 064617 (2011).
- [18] Y. Uozumi, T. Yamada, S. Nogamine, and M. Nakano, *Phys. Rev. C* **86**, 034610 (2012).
- [19] Y. Uozumi, T. Yamada, and M. Nakano, *J. Nuc. Sci. Tech.* **52**, 263 (2015).
- [20] Y. Uozumi, Y. Yamaguchi, G. Watanabe, Y. Fukuda, R. Imamura, M. J. Kobra, and M. Nakano, *Phys. Rev. C* **97**, 034630 (2018).
- [21] Y. Yariv, Th. Aoust, A. Boudard, J. Cugnon, J. C. David, S. Lemaire, and S. Leray, in *International Conference on Nuclear Data for Science and Technology* (EDP Sciences, Paris, 2008), p. 1125.
- [22] J. Cugnon and P. Henrotte, *Eur. Phys. J. A* **16**, 393 (2003).
- [23] M. Kawai, *Prog. Theor. Phys.* **27**, 155 (1961).
- [24] H. De Vries, C. W. De Jager, and C. De Vries, *At. Data Nucl. Data Tables* **36**, 495 (1987).
- [25] J. Cugnon, D. L. Hote, and J. Vandermeulen, *Nucl. Instr. Meth. B* **111**, 215 (1996).
- [26] N. J. DiGiacomo, R. M. DeVries, and J. C. Peng, *Phys. Rev. Lett.* **45**, 527 (1980).